





## Article

# Geological and Geomorphological Characterization of the Anthropogenic Landslide of Pie de la Cuesta in the Vitor Valley, Arequipa, Peru

Rosmery Infa <sup>1,\*</sup>, Antenor Chavez <sup>1</sup>, Jorge Soto <sup>1</sup>, Joseph Huanca <sup>1</sup>, Gioachino Roberti <sup>2</sup>, Brent Ward <sup>3</sup>, Rigoberto Aguilar <sup>4</sup> and Teresa Teixidó <sup>5</sup>

<sup>1</sup> Facultad de Geología, Geofísica y Minas, Universidad Nacional de San Agustín de Arequipa, Arequipa 04000, Peru; achavezv@unsa.edu.pe (A.C.); jsotov@unsa.edu.pe (J.S.); jhuancacard@unsa.edu.pe (J.H.)

<sup>2</sup> Mount Meager Consulting Inc., 17-38173 Westway Avenue, Squamish, BC V8B0Y4, Canada

<sup>3</sup> Department of Earth Sciences, Simon Fraser University, Burnaby, BC V5A1S6, Canada

<sup>4</sup> Instituto Geológico Minero y Metalúrgico, Dirección de Geología Ambiental y Riesgo Geológico, Arequipa 04000, Peru; aguilar\_rig@hotmail.com

<sup>5</sup> Instituto Andaluz de Geofísica y Prevención de Desastres Sísmicos, Universidad de Granada, 18071 Granada, Spain; tteixido@ugr.es

\* Correspondence: rinfaa@unsa.edu.pe

**Abstract:** This study presents the geological and geomorphological characterization of the Pie de la Cuesta landslide, a large (>60 ha) slow-moving (up 4.5 m/month) landslide in Southern Peru. The landslide has been active since 1975 and underwent a significant re-activation in 2016; the mass movement has caused the loss of property and agricultural land and it is currently moving, causing further damage to property and land. We use a combination of historical aerial photographs, satellite images and field work to characterize the landslide's geology and geomorphology. The landslide is affecting the slope of the Vitor Valley, constituted by a coarsening upward sedimentary sequence transitioning from layers of mudstone and gypsum at the base, to sandstone and conglomerate at the top with a significant ignimbrite layer interbedded within conglomerates near the top of the sequence. The landslide is triggered by an irrigation system that provides up to 10 L/s of water infiltrating the landslide mass. This water forms two groundwater levels at lithological transitions between conglomerates and mudstones, defining the main failure planes. The landslide is characterized by three main structural domains defined by extension, translation and compression deformation regimes. The extensional zone, near the top of the slope, is defined by a main horst–graben structure that transitions into the translation zone defined by toppling and disaggregating blocks that eventually become earth flows that characterize the compressional zone at the front of the landslides, defined by thrusting structures covering the agricultural land at the valley floor. The deformation rates range from 8 cm/month at the top of the slope to 4.5 m/month within the earth flows. As of May 2023, 22.7 ha of potential agricultural land has been buried.

**Keywords:** anthropogenic landslide; slow-moving landslide; irrigation-triggered mass movements; earth flow



**Citation:** Infa, R.; Chavez, A.; Soto, J.; Huanca, J.; Roberti, G.; Ward, B.; Aguilar, R.; Teixidó, T. Geological and Geomorphological Characterization of the Anthropogenic Landslide of Pie de la Cuesta in the Vitor Valley, Arequipa, Peru. *Geosciences* **2024**, *14*, 291. <https://doi.org/10.3390/geosciences14110291>

Academic Editor: Hans-Balder Havenith

Received: 16 May 2024

Revised: 22 October 2024

Accepted: 24 October 2024

Published: 31 October 2024



**Copyright:** © 2024 by the authors. Licensee MDPI, Basel, Switzerland. This article is an open access article distributed under the terms and conditions of the Creative Commons Attribution (CC BY) license (<https://creativecommons.org/licenses/by/4.0/>).

## 1. Introduction

This study focuses on characterizing the geomorphology and behavior of a large, slow-moving landslide [1,2] in the Vitor Valley, Arequipa, southern Peru. We applied field and remote sensing methods [3], including geomorphological mapping, stratigraphic survey, analysis of satellite and aerial images [4] and data from a geophysical investigation carried out by Huayllazo [5]. The objective of the study is to evaluate the dynamics, causes and reactivation mechanism of the landslide over time.

The article is structured as follows. The initial section describes the geological, geomorphological, structural and hydrogeological characteristics of the landslide (Section 3). The subsequent section provides a temporal analysis of satellite imagery (Section 4). The last sections present the discussions and results of the study (Sections 5 and 6).

### 1.1. The Vitor Valley

The Pie de la Cuesta landslide is located on the hydrological left flank of the Vitor River Valley in the Arequipa region, Southern Peru (Figure 1a), approximately 34 km to the west–southwest (WSW) of the city of Arequipa (Figure 1b). The Vitor River Valley has a northeast–southwest orientation, and resulted from the confluence of the Yura River and the Chili River valleys. Both valleys originate in the western foothills of the Peruvian Andes (Figure 1b) and flow towards the Pacific Ocean, incising up to 600 m canyons at the location of the landslide, in the Coastal cordillera (Figure 1b). The coastal cordillera is formed by the uplifting sedimentary fill of the Moquegua basin of the Cenozoic age [6] (Figure 1c). The Vitor River has a flow rate of 4 cubic meters per second during the dry season and increases to 50 to 100 cubic meters per second during the rainy season (from January to March).

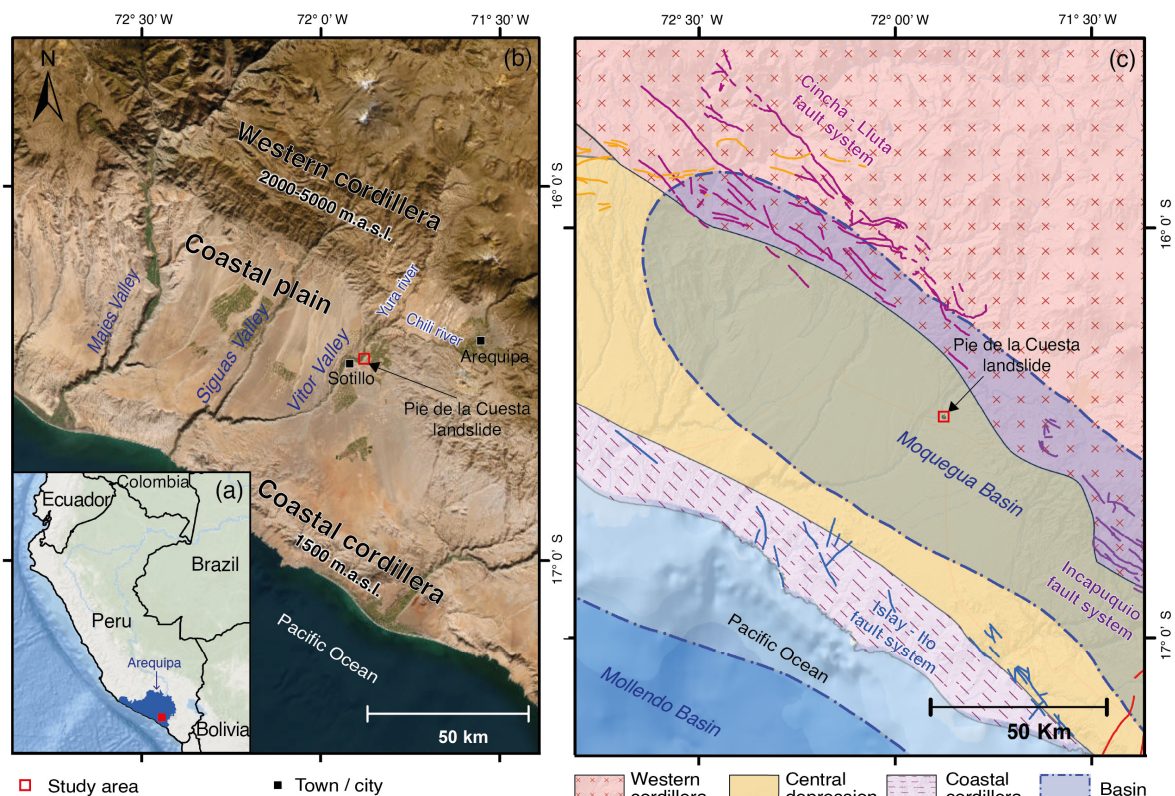


**Figure 1.** (a) Outline of the location of the study area (in red square). (b) Google Earth image showing the landslide location. (c) Regional geological units (modified from [7]).

### 1.2. Geology of the Vitor Valley

The Moquegua basin is an intramountain basin situated between the Coastal Cordillera to the west [7] (at approximately 1500 m above sea level) and the foothills of the Western Cordillera, ranging from 2000 to 5000 m above sea level. The Coastal Cordillera primarily consists of Precambrian metamorphic rocks intruded by Paleozoic and Mesozoic-age plutons. The Western Cordillera of the Peruvian Andes to the east is composed of Mesozoic sedimentary rocks with volcanic rock cover and continental sedimentary deposits. It is important to note that a batholith is in the western foothills of this cordillera, forming the western edge of the Moquegua Basin, as depicted in Figure 1c.

The sedimentary fill of the Moquegua Basin is primarily composed of materials eroded from the Western Cordillera. This fill is generally undisturbed but can sometimes be affected by reverse faults with steeply dipping strata and tectonic vergence toward the west, which are presented in Figure 1c. Moquegua Group deposits (~50 to 4 Ma) comprise mostly siliciclastic mudstones, sandstones and conglomerates as well as volcanic intercalations [8].

### 1.3. Landslides in the Vitor Valley

Gravitational landslides on valley walls are a relatively common geological process, contributing to the widening of valleys as rivers erode deeper into them. Landslides occurring on valley slopes due to the interplay of anthropogenic and geological factors represent an underlying issue in highly productive agricultural regions [9,10], leading to adverse social, economic and environmental consequences [11–15], particularly in areas with lithologies with poor geomechanics properties. Such is the case with the Pie de la Cuesta landslide in the Vitor Valley, Arequipa [5,16].

The controlling factors for landslides can be categorized as internal, which result in a decrease in the shear strength of slope components, and external, which result in an increase in the shearing stress [17]. In the context of the Pie de Cuesta landslide, internal factors [18] encompass poorly consolidated and cemented sediments (conglomerates), topography [19,20] and structural discontinuities. External factors [18] include heightened pore water pressure, fluctuations in groundwater levels, seismic events and disturbances resulting from human activities [20].

La Joya agricultural irrigation, covering over 3500 hectares, was initiated in 1938 [20]. About 12 years after the beginning of the irrigation systems, wet zones were documented on the Vitor Valley wall [20,21]. Currently, the irrigation system has a main concrete infrastructure; however, field irrigation still relies on earthen channels and flood irrigation.

The Pie de la Cuesta landslide was detected for the first time in 1974, and a significant collapse occurred on 9 January 1975 [20,22]. Since then, the landslide has had alternating periods of activity followed by periods of dormancy until sudden reactivation in 2016 [23]. Since the 2016 activation, the landslide has been consistently moving [20,23], affecting agricultural land in the valley plain [24].

Several other landslides can be observed in the Vitor Valley, including Punillo, La Cano, Huachipa and Boyadero (Table 1). These landslides are all related to irrigation systems on the plain at the top of the fluvial incision (Figure 2) [10,16,20]. These landslides cause damage to agricultural and civil infrastructure (roads, canals and agricultural land on the valley floor). Figure 2 shows the spatial distribution of the landslides that have significant horizontal displacements, all located on the slopes adjacent to La Joya Antigua, La Cano and San Isidro irrigation pampas. In 2019, these agricultural plots covered an approximate area of 105 km<sup>2</sup> [16]. All the triggering dates of the landslides have been around 20 years after the onset of the irrigation system [16] (Table 1).

**Table 1.** Geographical and historical data of the main landslides in the Vitor Valley.

Landslide	Location Latitude Longitude	Irrigation	Onsets of the Irrigation	Triggering Date	Reference
Pie de la Cuesta	16°27'44.20"S 71°52'33.13"O	La Joya Antigua	1953	1975	Ponce [22] 2008
Punillo	16°30'55.19"S 71°56'42.17"O	La Cano	1974	1990–2000	INGEMMET [25]
La Cano	16°32'35.50"S 71°57'46.92"O	La Cano	1974	1988–1995	Lacroix [16]
Huachipa	16°33'37.61"S 71°58'28.25"O	La Cano	1974	1988–1995	Lacroix [16]
Boyadero	16°34'40.09"S 71°59'11.08"O	La Cano	1974	1988–1995	Lacroix [16]

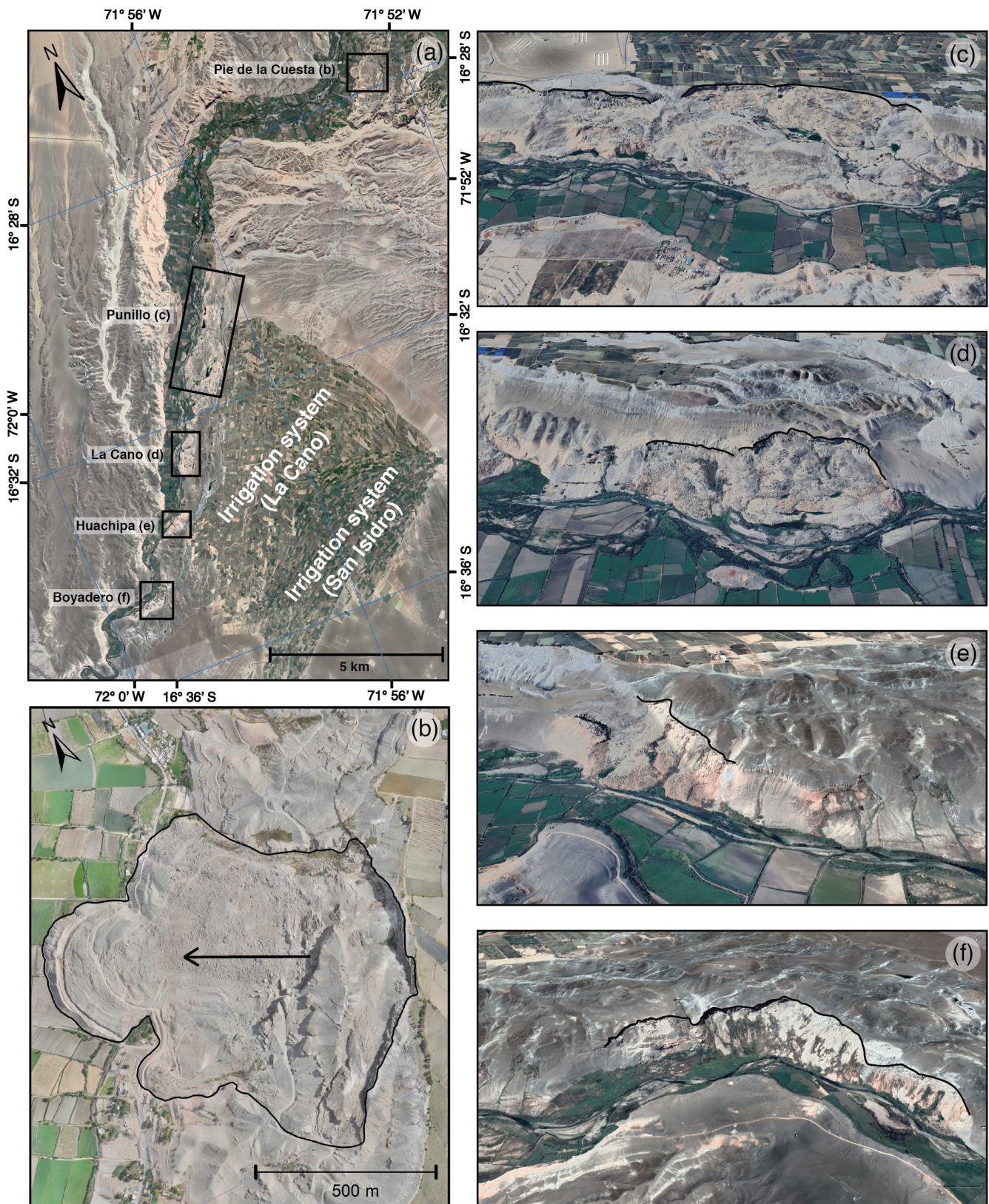


**Figure 2.** Google Earth images showing landslides in the Vitor Valley; black lines indicate landslides. (a) Geographical location of landslides in the valley and irrigation related to the landslides (b) Pie de la Cuesta Landslide, (c) Punillo Landslide, (d) La Cano Landslide, (e) Huachipa Landslide, (f) Boyadero Landslide.

## 2. Methods

Prior to field studies, a review of historical aerial photos and satellite imagery of the study area was conducted. Important landslide data such as measurements of landslide-related features, geomorphological observations prior to 1974 and before the 2016 reactivation, and hydrological information from other studies were extracted to assess the influence of water infiltration from irrigation on the landslide [26]. Field studies were also conducted to measure landslide-related characteristics [2] and gather geomorphological and geological information within the landslide and on stable slopes. Additionally, mapping of water seepages emerging at various levels was carried out. As a result, geomorphological and geological maps, as well as cross-sectional profiles, were obtained.

### 2.1. Historical Aerial Photos

For a better understanding of the landslide’s development, an aerial photograph from 1945 and a satellite image obtained from Google Earth in 2015 were used. The digitized version of the 1945 aerial map, sourced from the National Aerial Photographic Service, was georeferenced to the WGS84 coordinate system used for photogrammetry-generated products (Figure 3). To perform this adjustment, four control points were used, obtained from old buildings and geomorphological characteristics, with a margin of error of approximately 14 m. (Table 2). From this photo, it is possible to see that the hillside, before being affected by the landslide, was divided by three main ravines and the agricultural activity in the pampas of Joya Antigua. Likewise, a correlation was made with a georeferenced orthomosaic from May 2019 and two satellite images from October 2015 and May 2023.

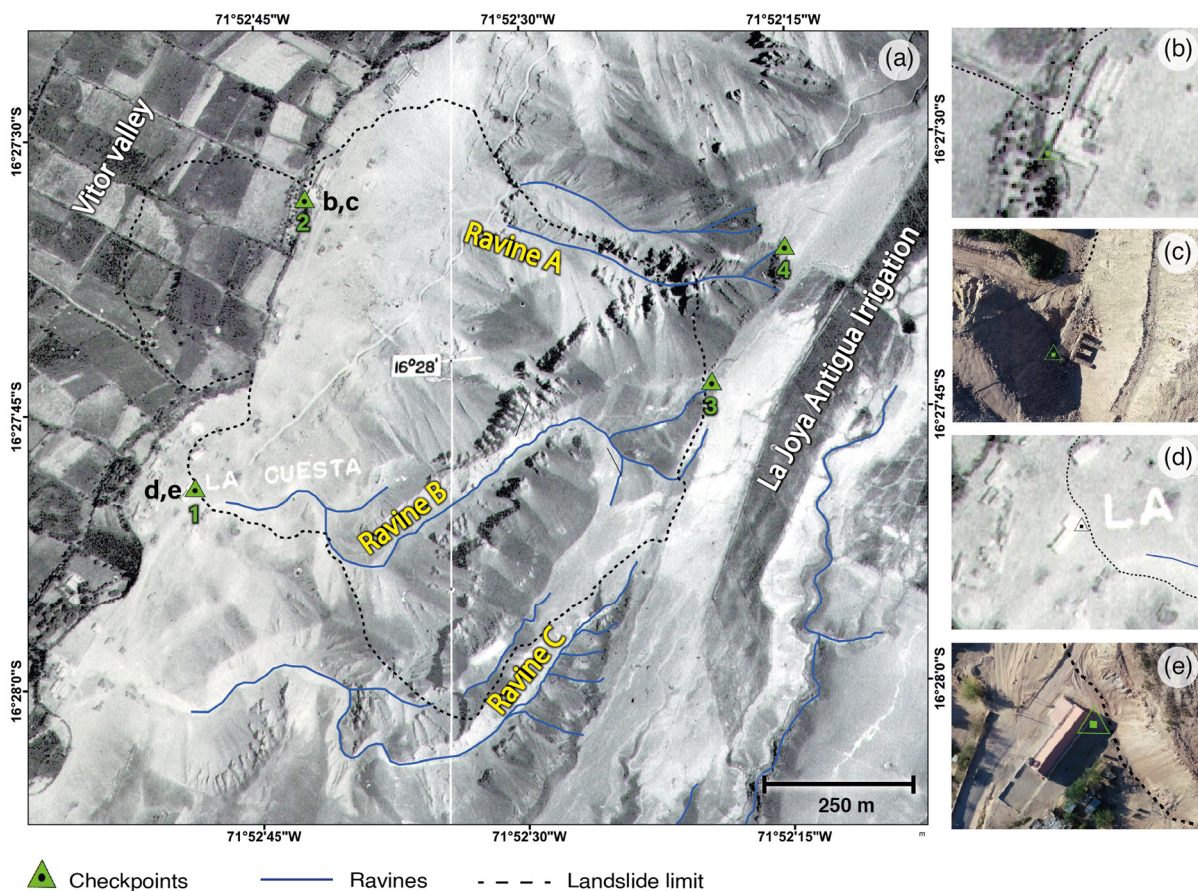


**Figure 3.** Aerial photograph from 1945 with the control points used for georeferencing. Numbers indicate control points.

**Table 2.** Detail of the control points used for georeferencing the aerial photograph. The total root mean square (RMS) error is 14 m [20].

Number	X Coordinates	Y Coordinates	Description
1	192459.34	8177590.25	Affected constructions
2	192643.02	8178075.04	Affected constructions
3	193326.35	8177769.20	Head of the ravine
4	193448.07	8177996.81	Head of the ravine

## 2.2. Satellite Imagery

For the analysis of the geomorphological context in which the landslide developed, current and historical satellite images extracted from Google Earth were utilized. These images enabled the assessment of how the terrain morphology has evolved over time, the identification of active displacement areas, regions with significant slopes, mapping of damaged or at-risk infrastructure due to landslides and the recognition of the types of mass movements occurring.

## 2.3. Field Mapping

The field study included the following. (1) Observations of the most relevant landslides in the Vitor Valley presented in Figure 2, to study the context in which the studied landslide develops. (2) Geomorphological observations and some measurements of morphometric characteristics of the landslide, such as spatial orientations and elevations, including main and secondary scarps, counter-scarps, horst–graben structures, cracks, side levee structures, etc. Water seepages were also mapped. This information was summarized in a geomorphological map. (3) Field mapping on the flanks of the landslide and stable slopes of the valley [27]. We identified and measured stratum thicknesses at rock outcrops and visually described hand samples to evaluate permeability, consolidation degree, grain size and texture, all aimed at assessing the influence of geological conditions of the strata on the landslide. Within the block, we particularly searched for fault planes with striations and any evidence of displacement to deduce the kinematics of the structures. Faults were mapped based on field measurements and analysis of satellite imagery and DEMs. As a result, a stratigraphic column and a structural geological map were obtained, and geological sections were generated by interpreting all collected data. USGS symbology was used for graphical representation.

## 2.4. Geophysical Survey Information

A 2D Electrical Resistivity Tomography (ERT) and 2D Seismic Vp Velocity (SVP) study of this landslide are presented by [5]. We use the electrical profile (ERT-01), the seismic profile (SVP-02) and a subsurface of the top of the Lower Moquegua formation by [5] to support our geological and geomorphological interpretations of the landslide.

## 3. Results

### 3.1. Stratigraphy

The stratigraphic units exposed in the study area range in age from the Eocene to the Quaternary period. These units correspond to the formations of Lower Moquegua, Upper Moquegua, Millo, Pleistocene alluvial deposits, Holocene terrace alluvial deposits and recent fluvial deposits [28,29]. Additionally, there are colluvial–deluvial deposits originating from landslides.

There is also an ignimbrite deposit, and Cenozoic volcanism occurred simultaneously with the sedimentation of the Millo Group [8]. The synthesized stratigraphic log is illustrated in Figure 4, which was logged on the right flank of the landslide.



### 3.1.1. Lower Moquegua Information (Sotillo)

The upper part includes red mudstones [30], and a noteworthy feature is a 4.5 m thick layer of coarse tuffaceous sandstones with centimeter-scale planar laminations as internal sedimentary structures (Figure 4j). The top of this unit comprises a 12 m thick layer of red mudstones, and within this layer, centimeter-sized gypsum spheres are present (Figure 4k). The upper boundary of this layer constitutes the detachment level of the landslide.

The middle part of this unit consists of meter-scale beds of silty mudstones with centimeter-thick gypsum layers. Fractures filled with gypsum, resulting from the dissolution of layers and subsequent precipitation as fracture infill, are also observed (Figure 4n). It also contains packages of impure white gypsum centimeter-thick layers that form scarps in the terrain. Some levels of mudstones with gypsum fragments produced during sedimentation are also present (Figure 4l).

The base of the Lower Moquegua Formation does not outcrop in the study area. It consists of lacustrine deposits composed of red mudstones and gypsum. At the base, there are fine alternations of red mudstones and centimeter-thick gypsum layers, creating irregular undulations developed during compaction due to lithostatic loading (Figure 4m).

The outcrop of this formation on the valley wall is part of the separation surface on which the landslide deposits rest (Figure 4b). The assigned age for this unit is Eocene.

### 3.1.2. Upper Moquegua Formation

This formation, with a thickness of 101 m, is underlain by an erosional discontinuity over the Sotillo Formation. It primarily consists of cream-colored polymictic conglomerates (Figure 4i). The clasts are rounded to subrounded, with a larger diameter ranging from 5 to 10 cm, although there are occasional clasts up to 20 cm. Clast lithology includes intrusive igneous rocks, sandstones and andesites, along with some limestones. The matrix is sandy, and sedimentary structures including channel structures are commonly observed. To a lesser extent, medium-to-coarse-grained cream-colored arkosic sandstones intercalate with inclined bedding structures, and there are metric layers of reddish-brown mudstones. This entire unit exhibits good cementation and morphologically forms multi-meter protruding prismatic features in the conglomerates (Figure 4g).

The sedimentary rocks of the Moquegua Group result from the erosion of the rocks that comprise the current Western Cordillera and the Altiplano [31].

The assigned age for this unit is Upper Oligocene to Miocene.

### 3.1.3. Millo Formation

The Millo Formation extensively outcrops in the study area, forming the upper part of the valley walls (Figure 4d). It is characterized by a dark gray color and overlies the Upper Moquegua formation with an erosional discontinuity. Lithologically, it is composed of rounded polymictic conglomerates with clasts varying in diameter from 5 to 10 and occasionally up to 20 cm. The clast lithology includes intrusive igneous rocks, sandstones and volcanic andesites, with a minor presence of limestones. The matrix is composed of coarse sand (Figure 4c), and the materials are weakly cemented, causing the clasts to detach easily and roll down the slope.

In the lower to middle part of the formation, there is an intercalated 5 m thick white ignimbrite deposit (Figures 4a and 5d). This is a tuff composed of volcanic ash, plagioclase crystals, biotite and scattered pumice clasts throughout the deposit. While the base of the deposit is relatively uniform, the upper part exhibits an erosional surface. The age of this deposit is  $4.89 \pm 0.02$  Ma [32], the same age assigned to the Millo Formation.



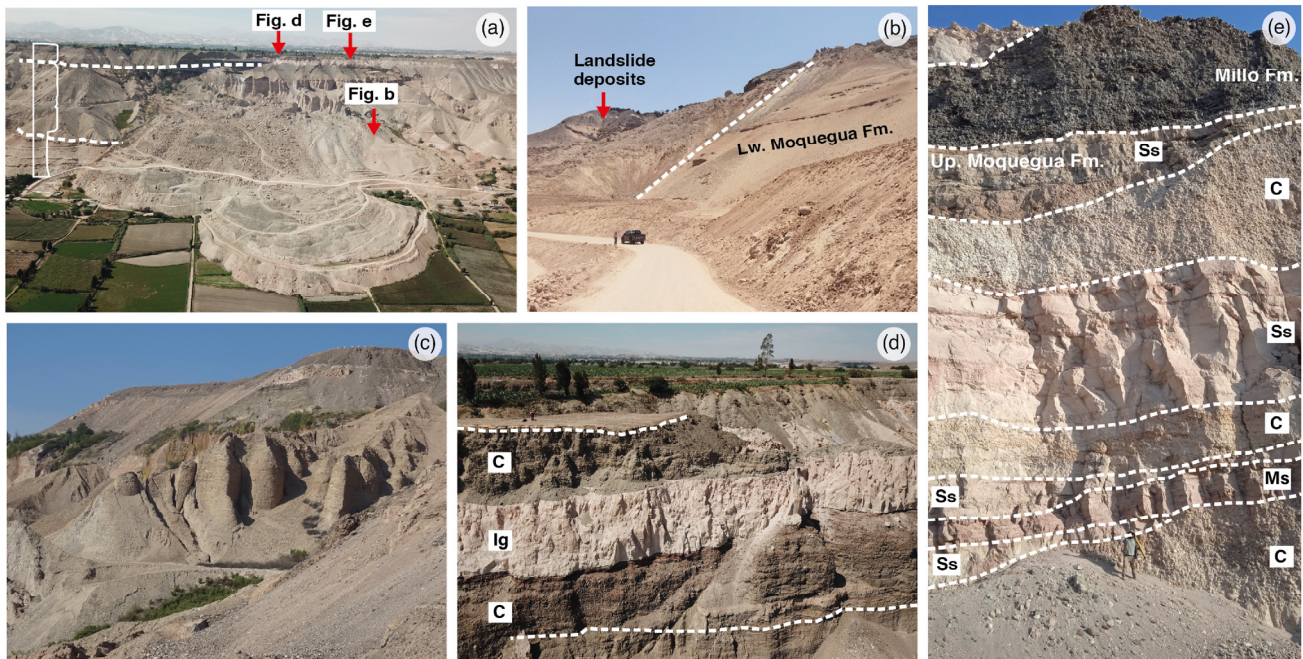


**Figure 5.** Field photographs showing (a) a panoramic view of Pie de la Cuesta landslide and locations of detail pictures (b,d,e); the stratigraphic sequence shown in Figure 4 is indicated by the white dashed line. (b) Southern limit of the landslide in contact with the sedimentary unit in the valley wall. (c) Erosional features in the conglomerates of the Upper Moquegua formation. (d) Outcrop on the main scarp of the landslide showing the top and base of the Millo formation, C conglomerate interbedded with Ignimbrite layer. (e) Outcrop of the Upper Moquegua Formation, showing interbedding of SS Sandstone, C Conglomerate and Ms Mudstone.

#### 3.1.4. Quaternary Deposits/Eolian Deposits/Farming and Irrigation

In the study area, the Millo Formation is covered by eolian deposits (Figure 6d) and soils (Figure 6c) that have been utilized for a farming area covering approximately 4500 hectares (Figure 6a,b). The irrigation system currently includes cement distribution canals, but the fields are irrigated primarily by flooding with earth channels. The water flow for irrigation ranges from 5 to 8 cubic meters per second [26].

#### 3.2. Geomorphology/Structures

The Pie de la Cuesta landslide is 1.07 km long and 0.78 km wide. At its head, the landslide exhibits a pseudo-graben structure, while at the bottom, there are blocks that have slid from the main wall. The most significant block preserves signs of cultivation and irrigation infrastructure. This pseudo-graben rests on an ancient ravine, at the bottom of which the materials cover the fault trace that initiates the landslide. In this study, four geomorphological subunits have been delimited (Figure 7).

Subunit (I) encompasses the landslide's initiation zone, featuring a main horst–graben structure with vertical to sub-vertical scarps identifying the horst and a collapsed graben approximately 50 m below the horst elevation. The graben walls experience rockfalls, and outcrop springs occur near the base. Remnants of agricultural fields with irrigation canals are visible on the graben surface (Figure 8a). This horst–graben structure was more active in the early stages of the landslide [20]; its subsidence has decreased to a minimum at present.



**Figure 6.** La Joya Antigua irrigation over Quaternary deposits. (a) A panoramic view of the head of the landslide showing Quaternary deposits. (b) Water channels for flood irrigation. (c) Quaternary deposits. (d) Eolian deposits. Red arrows indicate Quaternary deposits.

Additionally, within the depression (graben), cracks parallel to the direction of sliding can be observed, indicating lateral displacement of the landslide (Figure 8a). Associated with the main faults are antithetic faults that give rise to smaller grabens.

The horst has slid with primarily horizontal displacement and slight vertical movement (Figure 8a). The displacement is more pronounced on the NE side of the sliding block while maintaining the original stratigraphic configuration. Within the horst, there are north–south-trending cracks intersected by lesser-magnitude east–west-trending cracks.

Subunit (II): This subunit marks the initiation of earth flows, characterized by decameters tall toppling columnar blocks (Figure 8b) and multimeter-tall pyramidal blocks with vertical flanks and fault striations resulting from normal faulting (Figure 8c). This is the zone where the degree of deformation and disaggregation of the original sedimentary sequence increases from large blocks to the point of complete block disaggregation and generation of the debris that feeds the earth flows downstream.

Subunit (III): This zone consists of earth flows that originate at the contact between the Upper and Lower Moquegua formations. The flow path overlays an older ravine, valley wall and valley floor (Figure 3). The upper part corresponds to an area of hummocky topography composed of an agglomeration of blocks of sizes from 1 to 5 m, as well as boulders of centimetric sizes up to 50 cm. Side levee structures can be observed bounding the sides of the flows, while the front of the flows forms semicircular compressional ridges that define the advancing front of the landslide. This area exhibits the most mobility (up to 4.5 m/month) [20] and is currently advancing and covering agricultural land.

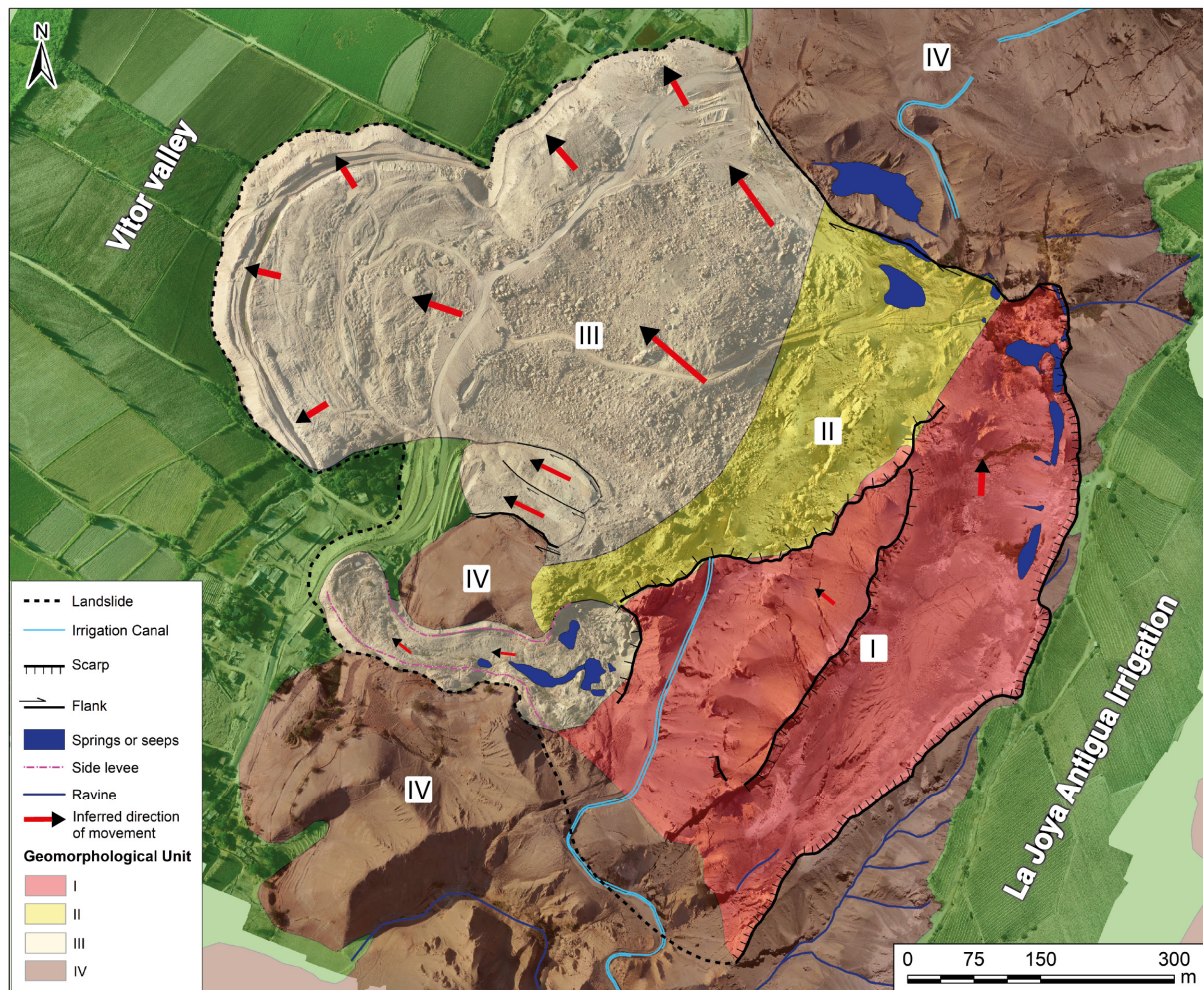


**Figure 7.** Geomorphological map of the Pie de la Cuesta landslide showing geomorphological domains: (I) horst–graben structure, (II) normal faulting and large pyramidal blocks, (III) earth flows, (IV) natural slope of the valley.

The landslide material slides along the natural slope developed in the Lower Moquegua Formation, as inferred from outcrops (Figure 5b) of the Lower Moquegua Formation on both sides of the landslide. The limited presence of Lower Moquegua material in the slid mass also supports this deduction. Additionally, aerial photos from 1945 (Figure 3), prior to the landslide, reveal the natural slope of the valley wall.

On the southern side, two water springs originating from the sliding plane (contact of the Lower and Upper Moquegua formations) are present. These springs become more active during periods of heavy rainfall and an increase in the irrigation water flow in the Joya region, triggering soil flow.

At the front of the landslide, reverse faults are observed in response to compression caused by the weight of the sliding mass. Striated fault planes are distinguishable (Figure 8c), as well as semicircular ridges that border the landslide front, resulting from the stacking of materials constrained by typical reverse faults characteristic of a landslide front (Figure 9). This zone covers agricultural lands with velocities ranging from 0.8 to 1.4 m/month [20], heading northwestward.

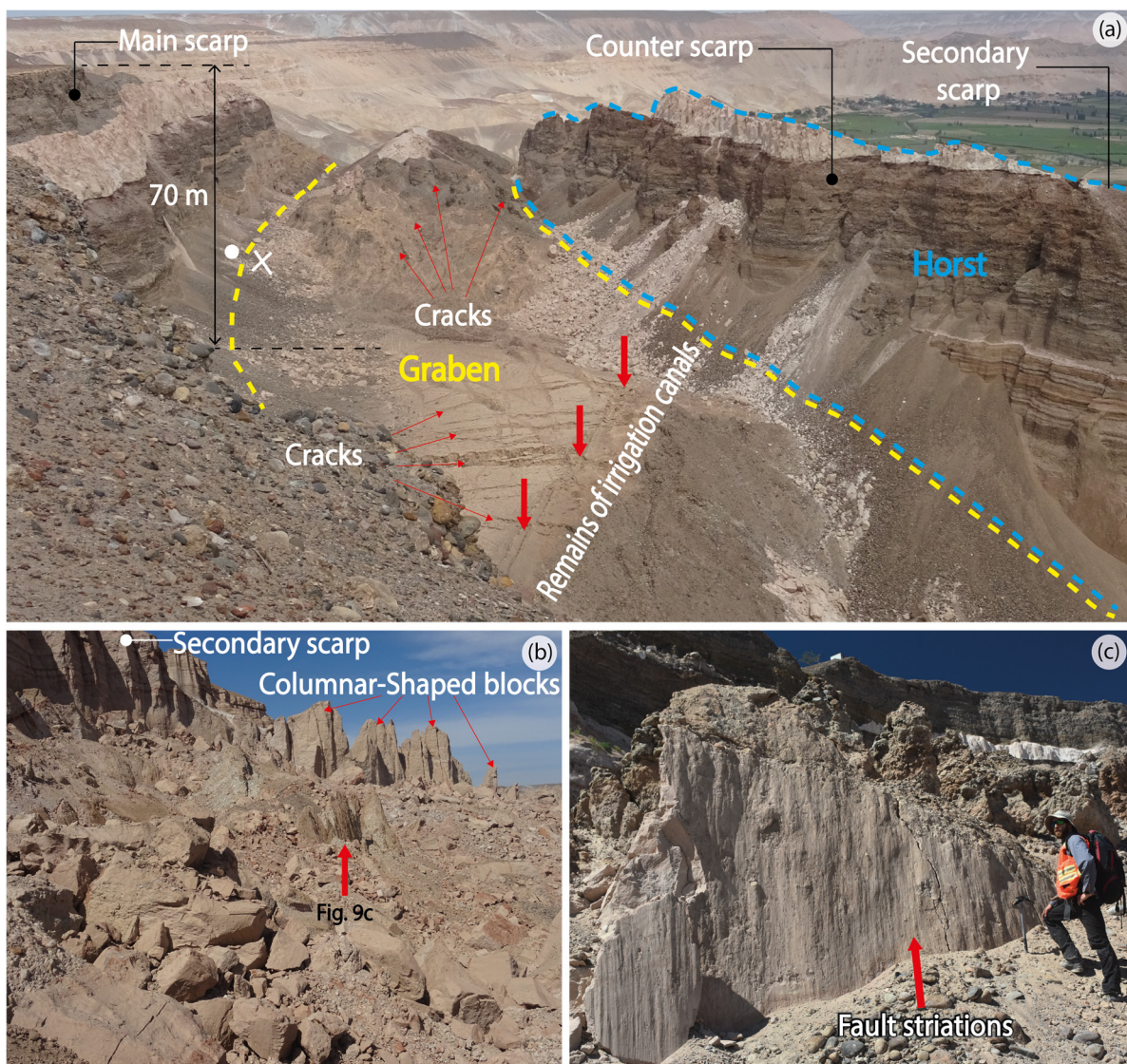


**Figure 8.** (a) Morphometric features observed in the landslide of Pie de la Cuesta. (b) Columnar-shaped blocks and scratched face. (c) Striated fault plane.

Moreover, considering the studied background and the monitoring data where the landslide developed [20], the order of occurrence of the earth flows and the average velocities are illustrated in Figure 10.

Subunit (IV): This refers to the stable areas around and within the landslide, where the original stratification is preserved.

Within the study area, various types of movements [33] contributing to the landslide's development have been identified, including block sliding, debris falling, rockfall, tipping and earth flows, which are illustrated in Figure 10.

The velocities of the earth flows vary in each zone due to factors such as valley morphology, irrigation water infiltration, material input and the composition of earth flows. Figure 10 presents the different velocities recorded during the period from October to November 2021 [20,23].

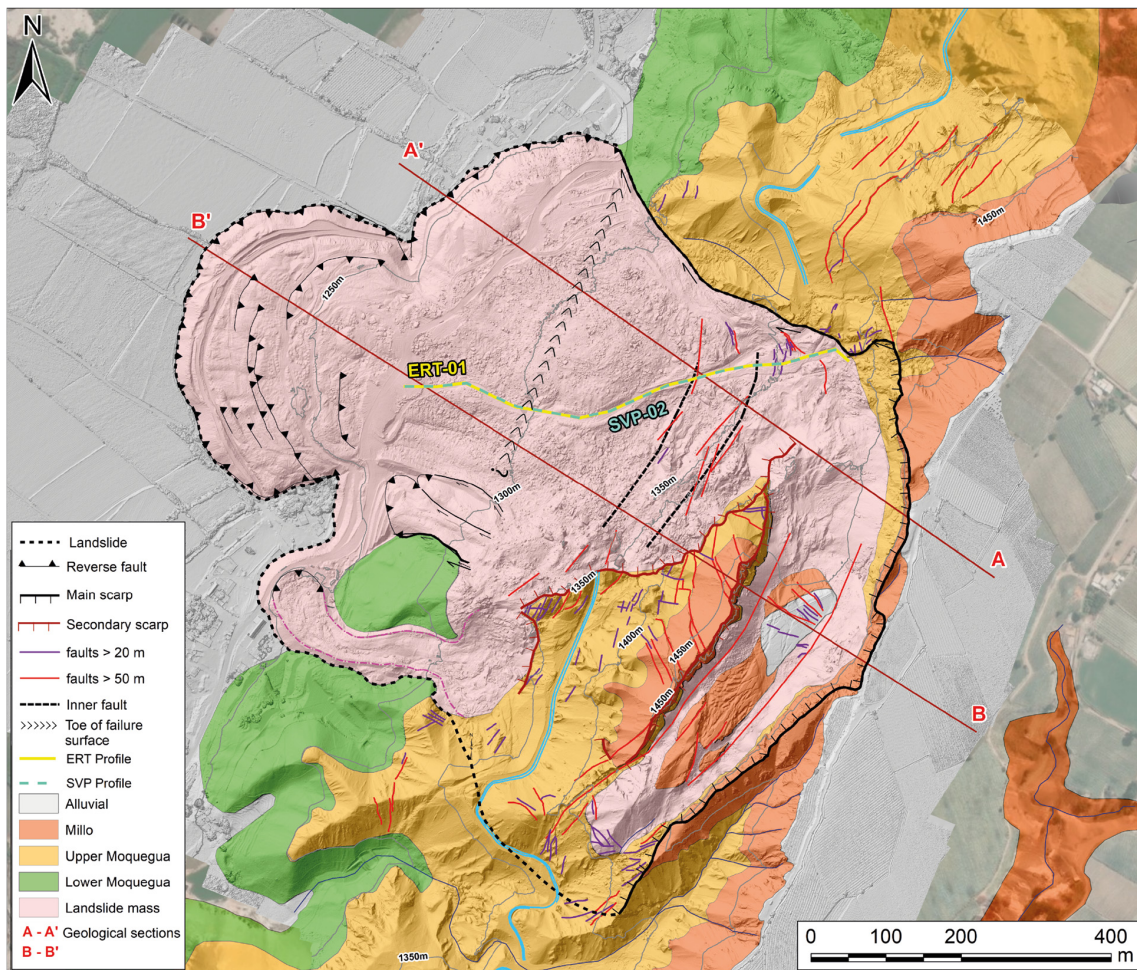


Figure 9. Geological and geomorphological map of the Pie de la Cuesta landslide. Faults, scarps, geophysical profiles, geological formations and landslide bodies are shown.

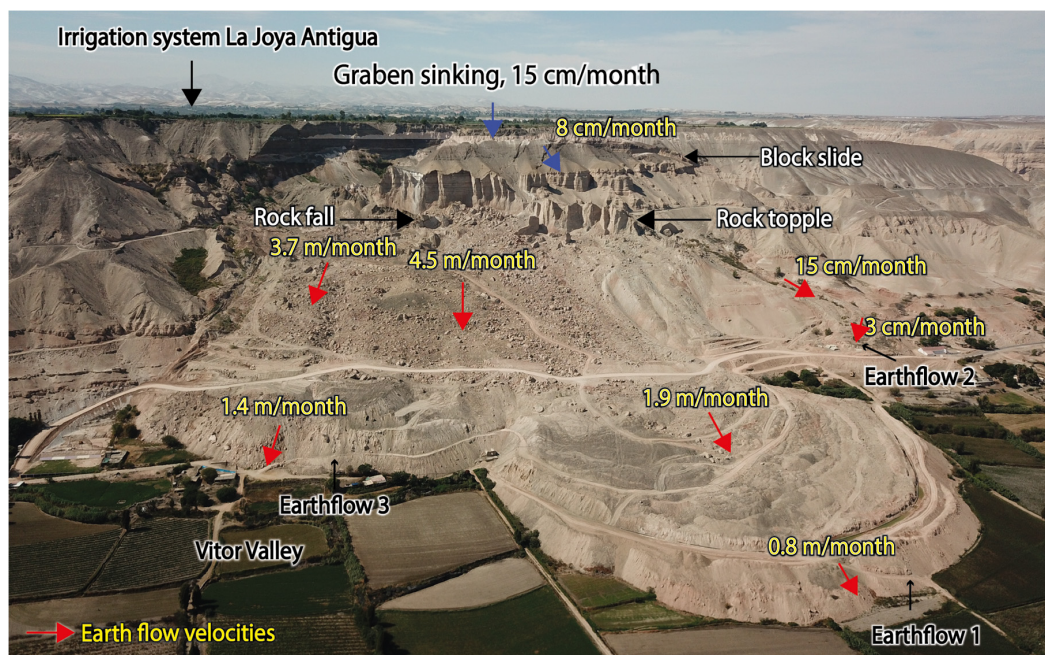
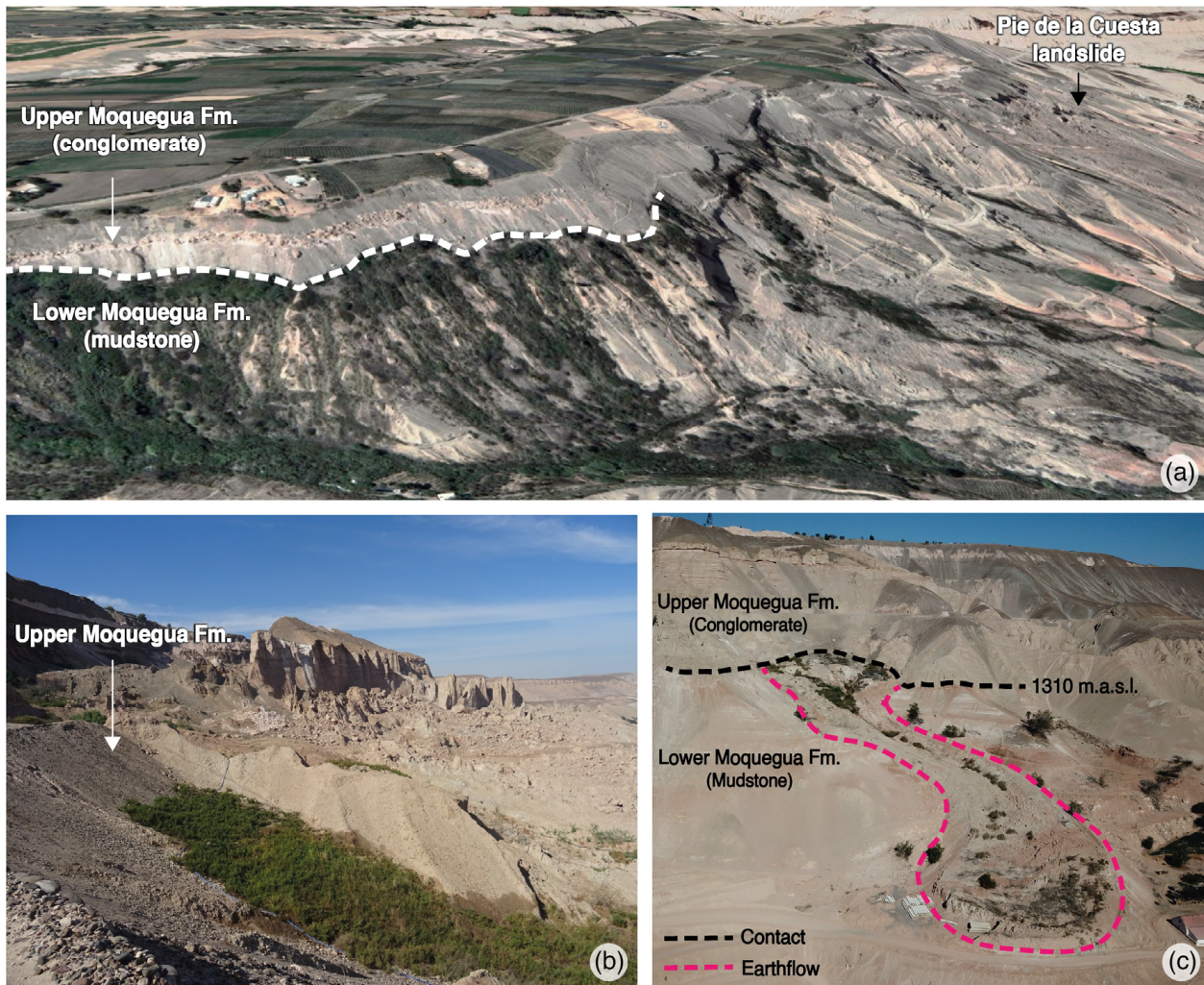


Figure 10. Earthflow movement rates [20] and types of movements [1].

### 3.3. Groundwater

The Pie de la Cuesta landslide is triggered by the Joya irrigation system [16,19,22,23]. The Joya irrigation system receives a flow of 5 m<sup>3</sup>/s in the dry season and up to more than 8 m<sup>3</sup>/s in the rainy season, and on average 7 m<sup>3</sup>/s [26]. Up to 10.5 (L/s), estimated from the discharge rate of the springs in the landslide body, infiltrates from the irrigation system the landslide mass [26]. The water electric conductance in the landslide was around 4.30 dS/m (decisiemens per meter) in 1994 [26]; this is due to the washing and dilution of minerals from the sedimentary units. These high-water electric conductance indices indicate the high salinity of aquifers. The salinity water may be due to the leaching of soils and rocks from the valley wall formations or the excessive use of fertilizers in La Joya Antigua irrigation.

Subsurface drainage flows toward the valley (Figure 11a), following a slight topographic slope of La Joya plains. This drainage emerges on the walls of the main escarpment, in the extensional area of the landslide and at the transition zone by the upper part of the earth flows.



**Figure 11.** Water outcrops at the contact between Millo and Upper Moquegua formation, along the left margin of the valley, 500 m downstream from the landslide. (a) Moisture zones. (b) Outcrop of water in the upper part of the flow. (c) Origin of earth flow at the contact between Upper Moquegua and Lower Moquegua formations.

Water infiltrates the sedimentary sequence both by primary permeability of the coarse sediments and by secondary permeability caused by fractures affecting the sedimentary units.

On the margins of the Vitor Valley, many springs of water are observed gushing from the cliffs, geographically related to the location of the irrigation fields [16], and controlled in turn mainly by geological conditions of the formations that outcrop on the walls of the valley [34].

In the study area, two main levels of water infiltration are observed. The first level of infiltration occurs from the main scarp, approximately 5 m below the contact between the upper Moquegua and Millo, although this level fluctuates downstream towards the contact itself; this is more visible 500 m downstream of the landslide and can be observed in the valley from Pie de la Cuesta to Boyadero along a distance of 15 km (Figure 11a). The second level of infiltration occurs at the contact between the Upper and Lower Moquegua formations, moist zones with the presence of vegetation on the north side of the landslide (Figure 11b) and on the south side with water springs at the top of the earth flow (Figure 11c).

#### 4. Deformation History and Interpretation of Structures

Based on the description provided, the factors controlling the landslide can be identified. The internal factors include the poorly consolidated conglomerates from the Millo and Upper Moquegua formations, which are a slightly fractured, permeable layer; the expansive nature of the mudstone interbedded with gypsum layers from the Lower Moquegua formation, impermeable layer and landslide surface; and the topographical conditions. The external factors comprise heightened pore water pressure, fluctuations in groundwater levels, seismic events and disturbances resulting from human activities [20]. However, the predominant triggering factor is water infiltration from La Joya Antigua area, supported by recorded instances of infiltration since approximately 1950 [20,21], the geographic association of landslides with farmland [16] and the mapping of springs or seeps (Figure 7).

La Joya Antigua flood irrigation systems span over 3500 hectares (Figure 6a,b). The irrigation water infiltrates the sedimentary sequence and outcrops of springs gushing from the cliffs of the Vitor Valley. Specifically, two levels of water infiltration have been detected along the left bank wall of the Vitor Valley.

The infiltrated water contains salts and minerals leached from the Millo and Upper Moquegua formations [5,35]. Groundwater flow directions on the subsurface of the top of the Lower Moquegua were drawn (Figure 12). Huayllazo et al. [5] extrapolated the point values of seven electrical profiles to obtain the subsurface of the top of the Lower Moquegua formation.

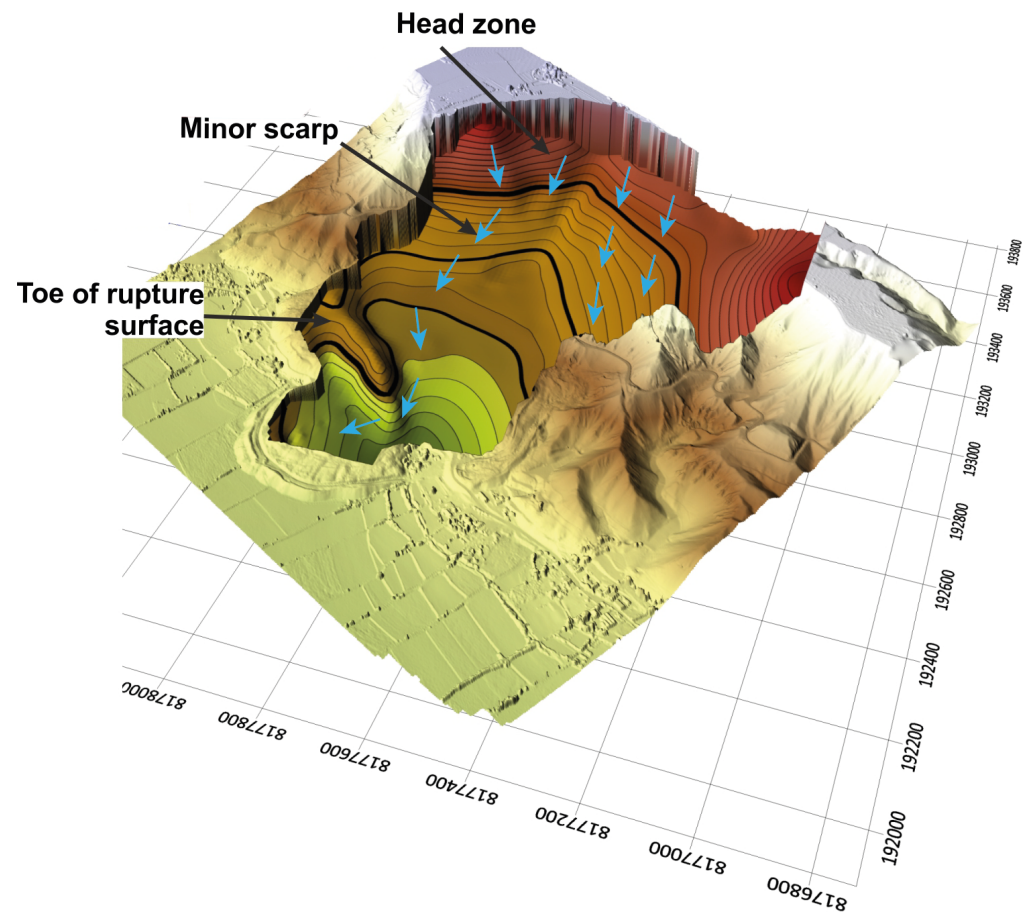


**Figure 12.** Failure surface under Digital Terrain Elevation model. The arrows indicate preferred groundwater flow directions. Modified from Huayllazo et al. [5].

The geological cross-sections A-A' and B-B' (Figure 13) are constructed from the topography obtained from the 2019 orthomosaic, geological field observations in 2019 and two geophysical profiles from Electrical Resistivity Tomography (ERT-01) and seismic refraction (SVP-02), extracted from a previously published study [5]. Interpreting the cross-sections B-B' (Figure 13), the upper part comprises the graben in which part of the soil has slid, along with its respective elevation with almost perpendicular fracturing to the sliding and affected at its southern end by normal faults, which attests to an initial sliding with a small rotational component. These two structural elements rest on a sub-horizontal sliding surface that joins the main sliding surface in the failure surface. This surface coincides with the contact between the Upper Moquegua (conglomerates) and the Lower Moquegua (red mudstones). The sliding surface follows the natural slope of the valley developed on the mudstones of the Lower Moquegua, as shown in Figure 13. Both sections illustrate inner faults that intersect the failure surface, which is also evidenced on the surface by the occurrence of normal faults. We refer to the area between inner faults such as the inflection zone, which has been delineated on the geological map (Figure 9).



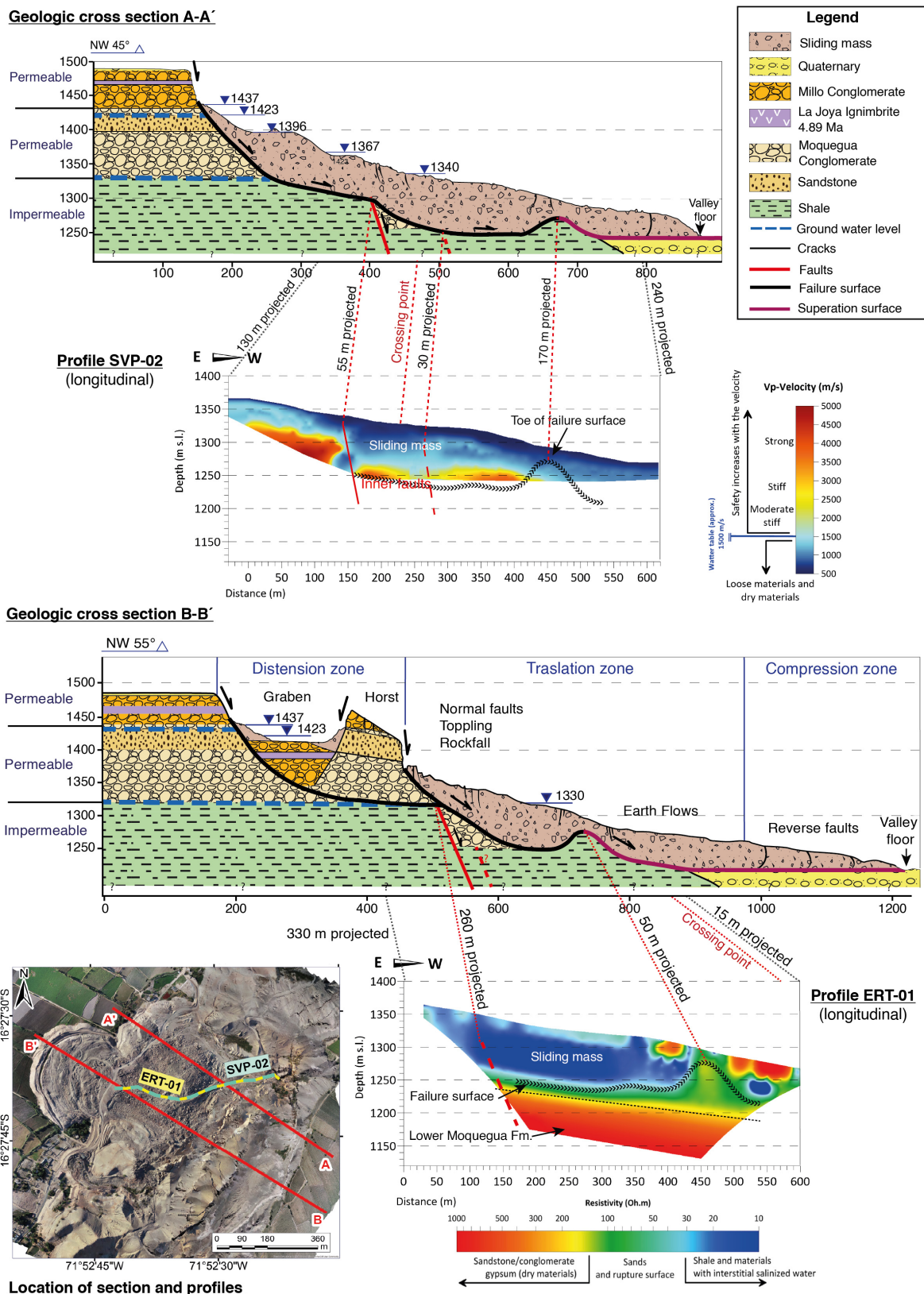


**Figure 13.** Geologic cross-sections obtained from surface geological mapping supported by one Electrical Resistivity Tomography line (ERT-01) and one Vp seismic refraction tomography line (SVP-02).

While Figure 3 shows the complex geomorphology of the terrain in the study area before being affected by the landslide in 1945, Figure 14 shows the state of the landslide two years after the main collapse that occurred in 1975 [19]. Source areas or contributory zones of the landslide are labeled in this figure. Zone Z1 shows the earth flows' source area, and a fractured block can also be observed, which would be the material that currently forms the earth flows covering the agricultural areas at the bottom of the valley. Additionally, zone Z2 is delineated, which is currently the secondary scarp of the landslide and part of the earth flows' source area. Consequently, zone Z3 is the main scarp of the landslide and could potentially become the main source area in the future when an external factor triggers a collapse of the horst structure, which is currently fractured in transverse and parallel directions to the direction of the landslide, as shown in Figure 9.

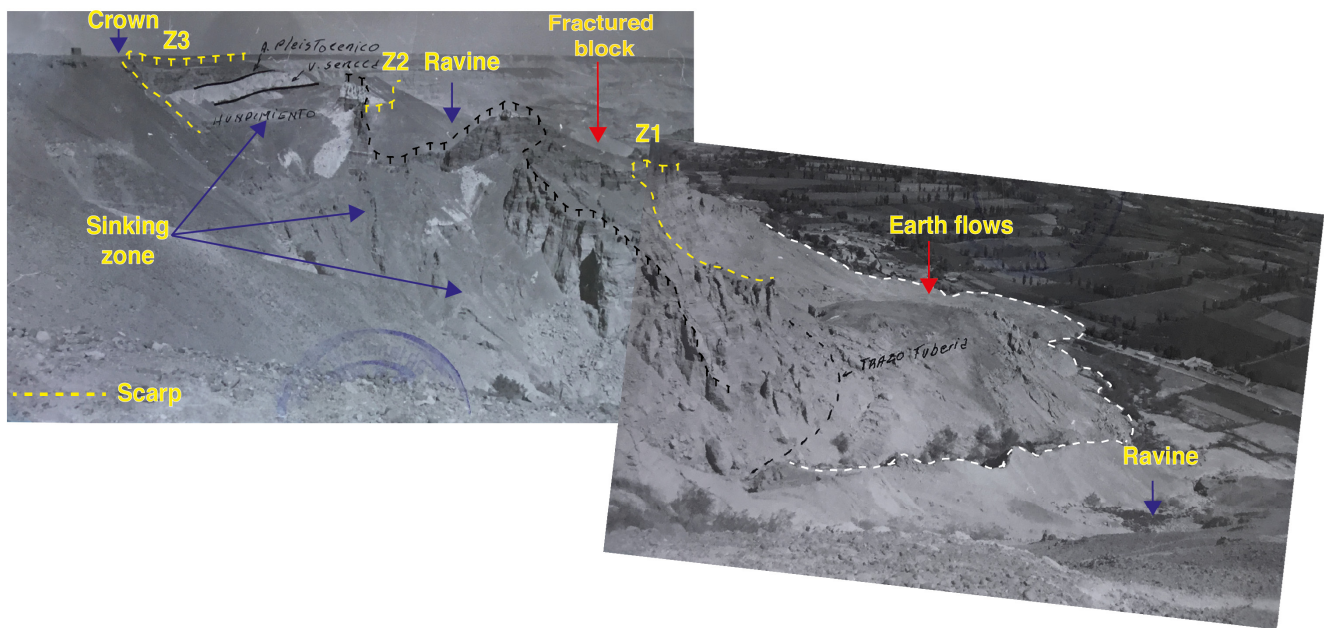


**Figure 14.** Photographs from 1977, two years after the main collapse, showing a 35 m sinking of the graben [19].

Figure 15 shows the historical evolution of the Pie de la Cuesta landslide. Figure 15a shows an aerial photo from 1945 showing the position of the foot of the slope in 1945 and the landslide boundary in May 2023, also the total buried area. Figure 15b shows a Google Earth satellite image from October 2015, showing the position of the foot of the landslide mass before reactivation in 2016. Figure 15c shows an aerial photo from 2019 showing the position of the foot of the landslide mass after reactivation.

The total buried area of the valley floor from the first activation in 1975 to October 2015 was approximately 15 hectares. From October 2015 to May 2019, after the reactivation in 2016, the buried area increased by 4.9 hectares. Finally, from May 2019 to May 2023, the increase in the buried area is 2.8 hectares. The total buried area on the valley floor due to the advance of the landslide mass until May 2023 is 22.7 hectares (Figure 15e).

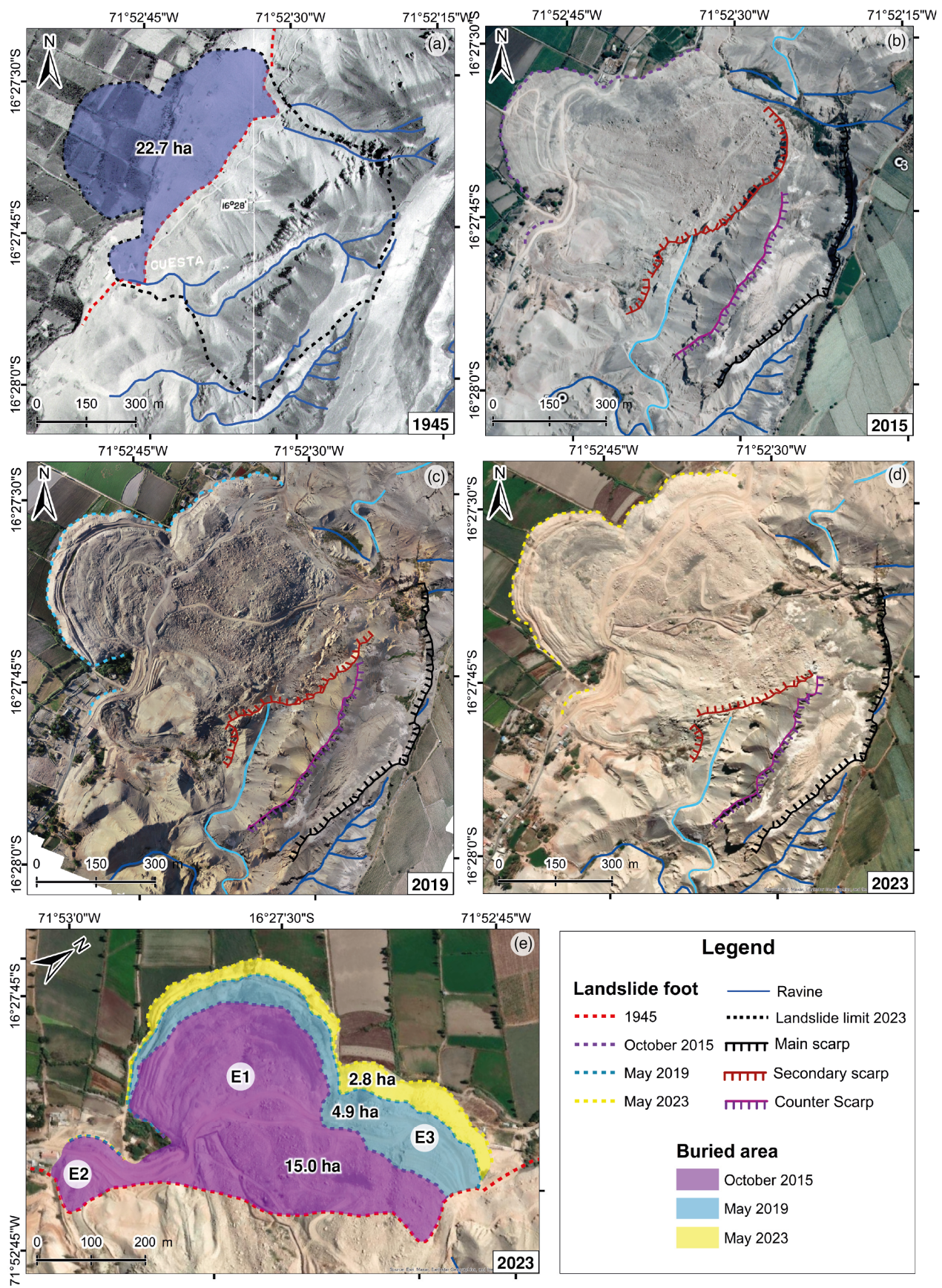


**Figure 15.** (a) Multitemporal evolution of the landslide by comparing geomorphological characteristics from aerial photos (a,c) and satellite images (b,d,e). (a) Aerial photo from 1945 showing

the position of the foot of the slope in 1945 (red dashed line) and the landslide boundary in May 2023. The blue polygon indicates the total buried area. (b) Google Earth satellite image from October 2015 showing the position of the foot of the landslide mass before reactivation. (c) Aerial photo from 2019 showing the position of the foot of the landslide mass after reactivation. (d) Google Earth satellite image from May 2023. (e) Position of the foot of the landslide, represented by dashed lines (2015–2023); the buried areas delimited at different time intervals are also shown.

## 5. Discussion

Taking into account the morphological, structural and hydrogeological characteristics illustrated in the profiles of Figure 13, it can be inferred that the failure surface (initiated by gravitational failure) is divided into two parts by an inflection zone.

The upper part comprises the graben in which part of the soil has slid, along with its respective irrigation infrastructure and underlying units, as observed in Figure 6a. The horst, with nearly perpendicular fracturing to the landslide and affected at its southern end by normal faults, attests to initial sliding with a small rotational component. These two structural elements rest on a sub-horizontal sliding surface that links to the main sliding surface in the break zone. This surface coincides with the contact between the Upper Moquegua (conglomerates) and the Lower Moquegua (red mudstones). It is crucial to note that this contact is an erosion surface with paleo-relief through which a groundwater level circulates. From the inflection zone, the sliding surface follows the natural slope of the valley developed over the mudstones of the Lower Moquegua, as depicted in Figure 13.

The lower part of the landslide, composed of the translation zone and the landslide front, represents most of the landslide volume. This greater mass of materials originated from an uplifted fractured block that was affected on its northwest flank by normal gravitational faults (Figure 14); the materials not only have undergone sliding but also experienced collapses, fracturing the materials of the Upper Moquegua and Millo Formations.

The mass in the translation zone exerts the greatest gravitational pressure forward, causing further advancement at the base of the landslide. This movement is also facilitated by the fact that the sliding surface in this zone has a steeper slope than the upper portion. It is worth noting that water emerging from the aquifers within the conglomerates of the Upper Moquegua, as well as those at the contact between the Upper and Lower Moquegua, infiltrates into the landslide materials and reaches the main sliding surface, acting as a lubricant.

The interbedded layers of permeable materials (Millo Formation and Upper Moquegua Formation) and nearly impermeable materials (Lower Moquegua Formation) (Figure 13) create concentrated flow zones at their contact, turning the contacts into failure areas. The presence of stratified permeable layers forms a groundwater level within the permeable stratum overlying the clayey soil, generating hydrodynamic pressures that vary with changes in water regime due to infiltration, leading to decreases in effective stresses. In other words, water infiltration circulates, exerting pore pressures on soil particles, which reduces effective stresses and consequently soil resistance, thereby forming a zone of weakness.

Local residents have installed a series of pipes and plastics to prevent water infiltration, but this mitigation effort is only partial. It is evident that water from flood irrigation in the Joya irrigation system infiltrates first into the Millo Formation, which is uncemented, highly porous, and permeable. Subsequently, it develops groundwater levels in the conglomerates and sands of the Upper Moquegua, even though this unit has moderate cementation, primarily composed of calcium carbonate and other highly soluble sulfates, allowing water circulation.

Displacement velocities in the translation zone vary considerably for the earth flows listed in order of occurrence in Figures 10 and 15e. The displacement velocity on average is 4 m/month in earth flow 3, 1.9 m/month in earth flow 1 and 15 cm/month in earth

flow 2 [20]. This movement is lower in the front due to the stacking of masses, generating reverse faults at the foot of the landslide. As of the date of this article, the landslide remains active since the involved mass has not yet been discharged and has not yet reached stability.

While it is true that the landslide is initiated by the destabilization of the valley wall due to the development of a slope through erosion [19], this movement is also facilitated by water infiltrating from the Joya irrigation system (over 3500 hectares) where flood irrigation is practiced. The water first infiltrates through the soil, then through the Millo Formation and continues to the Upper Moquegua Formation. Up to two main groundwater levels have developed, surfacing at the head of the landslide.

At the forefront of the landslide, there is a mass of landslide debris morphologically shaped like a fan, creeping over the valley floor. A series of semicircular ridges can be seen bordering it. Upon closer inspection in the field, these are overlapping flakes caused by reverse faults with striations on the fault planes.

The advance of the earth flows has buried approximately 22.7 ha of the valley floor, which implies damage to the infrastructure, such as a main access road, houses and irrigation canals (Figure 3) and the progressive loss of agricultural fields. On the other hand, the main road and irrigation pipes are located on the earth flows, generating economic losses in their recurring maintenance.

## 6. Conclusions

The study describes the geology and the geomorphology of the Pie de la Cuesta landslide using a combination of field and remote sensing methods and draws conclusions on the landslide cause and dynamics. Based on the information gathered in the research, the following conclusions can be drawn:

- The Pie de la Cuesta landslide was first identified in 1975, following an earthquake, and underwent a significant acceleration episode in 2016.
- Currently, the landslide covers approximately 61.5 hectares. The advance of the earth flows has buried approximately 22.7 ha of the valley floor, burying agricultural fields and infrastructure.
- The Pie de la Cuesta landslide is triggered by the presence of groundwater levels due to infiltrated water originating from La Joya Antigua irrigation system.
- The poor cementation of the conglomerates of the Millo and Upper Moquegua formations are key conditioning factors in the landslide failure and movement.
- The landslide is characterized by three deformation domains: an extensional domain defined by a horst–graben structure near the top of the valley slope; a translational domain defined by toppling, normal faulting and earth flows; and a compressional domain defined by lobed thrust fault ridges overtopping the valley bottom.
- It is a complex landslide as it exhibits different types of movements, including falls, topples, translational slides and earth flows.
- From the collected hydrogeological information, two main levels of infiltration water discharge are distinguished. The first occurs on the main scarp in the conglomerates of the Upper Moquegua Formation, approximately near the contact between the Millo and Moquegua Formations. The second level is at the contact between the Upper and Lower Moquegua Formations. It is noteworthy that mapped emergence points at different levels than those mentioned before lead to the conclusion that water also infiltrates through the sliding plane, thereby accelerating its progression. Due to the development of groundwater levels, the slope of the valley is 25 to 30 degrees, influenced by geological conditions such as the poor cementation and permeability of the formations on the upper part of the slope.
- The main failure plain develops at the contact between the Upper Moquegua Formation (conglomerates) and the Lower Moquegua Formation where the low-permeability mudstones of the Lower Moquegua Formation identify the main failure and sliding plane.

We advise the implementation of landslide monitoring and a strategy for improving irrigation practices to reduce the impact of the Pie de la Cuesta landslide and the other landslides in the Vitor Valley.

**Author Contributions:** Conceptualization, A.C. and J.S.; methodology, G.R. and B.W.; software, R.I. and J.H.; validation, G.R., R.A. and J.H.; resources, R.I., J.H. and G.R.; writing—review and editing, R.I., A.C., J.S., G.R., R.A. and J.H.; supervision, T.T., A.C., J.S. and R.A. All authors have read and agreed to the published version of the manuscript.

**Funding:** This research was funded by the Perú National Research Program funding the National University of San Agustín of Arequipa to carry out the Research Project grant number IBAIB-03-2018-UNSA. The APC was funded by the National University of San Agustín of Arequipa.

**Data Availability Statement:** Data are contained within the article.

**Acknowledgments:** The authors acknowledge Enrique Laura, for his important contribution to their writing, and the National University of San Agustín of Arequipa for funding the fieldwork.

**Conflicts of Interest:** The authors declare that they have no known competing financial interests or personal relationships that could have appeared to influence the work reported in this paper.

## References

- Hungr, O.; Leroueil, S.; Picarelli, L. The Varnes classification of landslide types, an update. *Landslides* **2014**, *11*, 167–194. [CrossRef]
- Gaidzik, K.; Žaba, J.; Ciesielczuk, J. Tectonic control on slow-moving Andean landslides in the Colca Valley, Peru. *J. Mt. Sci.* **2020**, *17*, 1807–1825. [CrossRef]
- Segoni, S.; Barbadori, F.; Gatto, A.; Casagli, N. Application of Empirical Approaches for Fast Landslide Hazard Management: The Case Study of Theilly (Italy). *Water* **2022**, *14*, 3485. [CrossRef]
- Peternel, T.; Janža, M.; Šegina, E.; Bezak, N.; Maček, M. Recognition of Landslide Triggering Mechanisms and Dynamics Using GNSS, UAV Photogrammetry and In Situ Monitoring Data. *Remote Sens.* **2022**, *14*, 3277. [CrossRef]
- Huayllazo, Y.; Infa, R.; Soto, J.; Lazarte, K.; Huanca, J.; Alvarez, Y.; Teixidó, T. Using Electrical Resistivity Tomography Method to Determine the Inner 3D Geometry and the Main Runoff Directions of the Large Active Landslide of Pie de Cuesta in the Vitor Valley (Peru). *Geosciences* **2023**, *13*, 342. [CrossRef]
- Alvan, A.; Eynatten, H.V. Sedimentary facies and stratigraphic architecture in coarse-grained deltas: Anatomy of the Cenozoic Camaná Formation, southern Peru (16°25' S to 17°15' S). *J. South Am. Earth Sci.* **2014**, *54*, 82–108. [CrossRef]
- Alvan, A.; Criales, A.; Eynatten, H.V.; Dunkl, I.; Gerdes, A.; Jacay, J. Seismic-stratigraphic architecture of the Oligocene-Pliocene Camaná Formation, southern Peruvian forearc (Province of Arequipa). *Andean Geol.* **2017**, *44*, 17–38. [CrossRef]
- Decou, A.; Von Eynatten, H.; Mamani, M.; Sempere, T.; Wörner, G. Cenozoic forearc basin sediments in Southern Peru (15–18 S): Stratigraphic and heavy mineral constraints for Eocene to Miocene evolution of the Central Andes. *Sediment. Geol.* **2011**, *237*, 55–72. [CrossRef]
- García-Chevesich, P.; Wei, X.; Ticona, J.; Martínez, G.; Zea, J.; García, V.; Alejo, F.; Zhang, Y.; Flamme, H.; Graber, A.; et al. The Impact of Agricultural Irrigation on Landslide Triggering: A Review from Chinese, English, and Spanish Literature. *Water* **2021**, *13*, 10. [CrossRef]
- Araujo, G.; Valderrama, P.; Taipei, E.; Miranda, R. *Dinámica y Monitoreo del Deslizamiento de Sigvas. Región Arequipa, Provincia Caylloma y Arequipa, Distrito Majes y San Juan de Sigvas*; Technical, Report; N°, A6748; Región Arequipa, Provincia Arequipa; Instituto Geológico, Minero y Metalúrgico: Arequipa, Perú, 2017. Available online: <https://repositorio.ingemmet.gob.pe/handle/20.500.12544/791> (accessed on 10 May 2024).
- Schuster, R.L. Socioeconomic and environmental impacts of landslide. In *Landslides Investigation and Mitigation*, 1st ed.; Turner, A.K., Schuster, R.L., Eds.; Transportation Research Board: Washington, DC, USA; Citeseer: Princeton, NJ, USA, 1996; Volume 247, pp. 12–35.
- Froude, M.J.; Petley, D.N. Global fatal landslide occurrence from 2004 to 2016. *Nat. Hazards Earth Syst. Sci.* **2018**, *18*, 2161–2181. [CrossRef]
- Butcher, B.; Walton, G.; Kromer, R.; Gonzales, E.; Ticona, J.; Minaya, A. High-Temporal-Resolution Rock Slope Monitoring Using Terrestrial Structure-from-Motion Photogrammetry in an Application with Spatial Resolution Limitations. *Remote Sens.* **2024**, *16*, 66. [CrossRef]
- Hou, X.; Vanapalli, S.K.; Li, T. Water infiltration characteristics in loess associated with irrigation activities and its influence on the slope stability in Heifangtai loess highland, China. *J. Eng. Geol.* **2018**, *234*, 27–37. [CrossRef]
- Yang, J.; Shragge, J.; Girard, A.J.; Gonzales, E.; Ticona, J.; Minaya, A.; Krahenbuhl, R. Seismic Characterization of a Land-slide Complex: A Case History from Majes, Peru. *Sustainability* **2023**, *15*, 13574. [CrossRef]
- Lacroix, P.; Dehecq, A.; Taipei, E. Irrigation-triggered landslides in a Peruvian desert caused by modern intensive farming. *Nat. Geosci.* **2020**, *13*, 56–60. [CrossRef]

17. Cotecchia, F.; Santaloia, F.; Tagarelli, V. Towards A Geo-Hydro-Mechanical Characterization of Landslide Classes: Preliminary Results. *Appl. Sci.* **2020**, *10*, 7960. [[CrossRef](#)]
18. Terzaghi, K. Mechanism of landslides. In *Application of Geology to Engineering Practice (Berkeley Volume)*; Geological Society of America: Washington, DC, USA, 1950; pp. 83–123.
19. Huerta, V. Rehabilitation of the Moco Canal—San Luis in the Pie de la Cuesta Section—La Cano Irrigation—Geological and Geotechnical Study. Licentiate Thesis, National University of San Agustín of Arequipa, Arequipa, Peru, 1977.
20. Huanca, J. *Aplicación de la Técnica GNSS-RTK y la Fotogrametría con Drones para la Caracterización y el Monitoreo del Deslizamiento de Tierra Activo de pie de la Cuesta en el Valle de Vitor, Arequipa*; Universidad Nacional de San Agustín de Arequipa: Arequipa, Peru, 2022.
21. Flores, A.; Maggiolo, O. *Reconocimiento Geotécnico de la Margen Izquierda del Río Vitor en el Sector Donde se han Presentado Deslizamientos que Afectan el Canal de Riego La Cano y el Poblado Pie de la Cuesta*; Preliminary Technical Report No. 001-75-IIA-IG; Department of Agriculture: Arequipa, Peru, 1975.
22. Ponce, V.A. Impacto Hidrológico y Ambiental de las Irrigaciones de La Joya y San I-idro—La Cano en el Valle de Vitor, Arequipa, Perú. Available online: [https://ponce.sdsu.edu/vitor\\_impacto\\_hidrologico\\_01.html](https://ponce.sdsu.edu/vitor_impacto_hidrologico_01.html) (accessed on 24 December 2023).
23. Araujo, G.E.; Miranda, R. *Evaluación Geológica y Geodinámica de Deslizamientos en el Flanco Izquierdo del Valle de Vitor, Sectores Pie de la Cuesta, Telaya, Gonzales y Socabón. Distritos Vitor y La Joya, Región Arequipa, Provincia Arequipa*; INGEMMET: Lima, Perú, 2016; Available online: <https://hdl.handle.net/20.500.12544/1165> (accessed on 5 June 2024).
24. Griffiths, J. Proving the occurrence and cause of a landslide in a legal context. *Bull. Int. Assoc. Eng. Geol.* **1999**, *58*, 75–85. [[CrossRef](#)]
25. INGEMMET. Evolución y Monitoreo Fotogramétrico del Deslizamiento de Punillo Periodo 2020. Región Arequipa, Provincia Arequipa, Distritos La Joya, Vitor. Available online: <https://repositorio.ingemmet.gob.pe/handle/20.500.12544/2653> (accessed on 15 March 2024).
26. Mansilla, D.; Neyra, M. Análisis de la Relación del Sobre Riego en las Irrigaciones La Joya Antigua y la Joya Nueva, con los Caudales de Retorno y los Deslizamientos Rotacionales en el Valle de Vitor. Licentiate Thesis, Catholic University of Santa Maria, Arequipa, Peru, 2022.
27. McClay, K.R. *Mapping Techniques*; Handbook Series—The Mapping of Geological Structures; Geological Society of London: London, UK; John Wiley: Hoboken, NJ, USA, 1987; pp. 17–44.
28. Marocco, R. Dynamique du remplissage d’un bassin intramontagneux cénozoïque andin: Le bassin Moquegua (Sud du Pérou). *Cah. ORSTOM. Série Géologie* **1984**, *14*, 123–129. Available online: <https://app.ingemmet.gob.pe/biblioteca/pdf/Reg-216.pdf> (accessed on 7 May 2024).
29. Bellido, E. Geología del Cuadrángulo de Moquegua, Hoja: 35-u (Boletín A 15). *INGEMMET* **1979**. Available online: [https://repositorio.ingemmet.gob.pe/bitstream/20.500.12544/132/3/A015-Boletin\\_Moquegua-35u.PDF](https://repositorio.ingemmet.gob.pe/bitstream/20.500.12544/132/3/A015-Boletin_Moquegua-35u.PDF) (accessed on 10 May 2023).
30. Underwood, L.B. Classification and identification of shales. *J. Soil. Mech. Found. Div. Proc. Am. Soc. Civil. Eng.* **1967**, *93*, 97–116. [[CrossRef](#)]
31. Sempere, T.; Jacay, J.; García, F. Elementos para una actualización de la estratigrafía del Grupo Moquegua, sur del Perú. *Boletín Soc. Geológica Perú* **2015**, *110*, 71–75.
32. Paquereau-Lebti, P.; Thouret, J.C.; Wörner, G.; Fornari, M. Neogene and Quaternary ignimbrites in the area of Arequipa, Southern Peru: Stratigraphical and petrological correlations. *J. Volcanol. Geotherm. Res.* **2006**, *154*, 251–275. [[CrossRef](#)]
33. Cruden, D.M.; Varnes, D.J. Landslide types and processes, special report, transportation research board. *Nat. Acad. Sci.* **1996**, *247*, 36–71.
34. Lee, J.-U.; Cho, Y.-C.; Kim, M.; Jang, S.-J.; Lee, J.; Kim, S. The Effects of Different Geological Conditions on Landslide-Triggering Rainfall Conditions in South Korea. *Water* **2022**, *14*, 2051. [[CrossRef](#)]
35. Baldys, S., III; Ham, L.K.; Fossum, K.D. *Summary Statistics and Trend Analysis of Water-Quality Data at Sites in the Gila River Basin, New Mexico and Arizona*; US Department of the Interior, US Geological Survey: Washington, DC, USA, 1995. Available online: <https://pubs.usgs.gov/wri/1995/4083/report.pdf> (accessed on 15 June 2023).

**Disclaimer/Publisher’s Note:** The statements, opinions and data contained in all publications are solely those of the individual author(s) and contributor(s) and not of MDPI and/or the editor(s). MDPI and/or the editor(s) disclaim responsibility for any injury to people or property resulting from any ideas, methods, instructions or products referred to in the content.